Journal of Materials Chemistry

Dynamic Article Links

Cite this: *J. Mater. Chem.*, 2011, **21**, 18983

www.rsc.org/materials

**PAPER**

# Enhanced one dimensional mobility of oxygen on strained $LaCoO_3$(001) surface

**Jeong Woo Han and Bilge Yildiz***

***Received 20th June 2011, Accepted 5th August 2011***
**DOI: 10.1039/c1jm12830b**

Mechanisms by which lattice strain alters the oxygen reduction reaction (ORR) kinetics are important to understand in order to increase the ORR activity of solid oxide fuel cell cathodes. Here we assess the mechanistic and quantitative effects of strain on oxygen diffusion on the $LaCoO_3$(LCO)(001) surface using density functional theory calculations. Planar tensile strain is found to reduce the migration barrier of oxygen vacancy anisotropically on the LCO(001) surface, inducing an enhanced mobility along the [1$\bar{1}$0] direction and a suppressed mobility along the [110] direction. The increase of space around Co that the oxygen (vacancy) traverses with a curved path is the cause of the enhanced mobility along the [1$\bar{1}$0]. The increasing octahedral distortions with planar tensile strain inhibit the migration of oxygen vacancy along the [110] direction. Furthermore, the mobility of the adsorbed oxygen atom is suppressed with increasing strain due to its stronger adsorption on the surface. On the basis of rate theory estimates, the significantly lower energy barrier for oxygen vacancy diffusion is expected to dominate the other degrading factors and actually accelerate the ORR kinetics on LCO(001) up to 3% strain. The insights obtained here are useful for designing strategies to control the desired anisotropic and uni-directional oxygen transport along strained hetero-interfaces.

## 1. Introduction

Discovery of highly active cathode materials for oxygen reduction in solid oxide fuel cells (SOFC) at intermediate temperatures (500–700 °C) remains an important challenge for improving materials stability and system cost.[1–4] This requires an improved understanding of the oxygen reduction reaction (ORR) mechanism at the molecular level, and of the underlying correlation between the ORR kinetics and the inherent structure of the cathode materials. Experimental studies probing the surface catalytic properties of cathode materials, in particular the oxygen surface exchange coefficients, have identified important information about the collective behavior of ORR kinetics.[5–10] First-principles based calculations, within the approximation frameworks as density functional theory (DFT) calculations, on the other hand, can uncover the mechanisms and kinetics of the elementary steps of ORR, and how the kinetic descriptors of ORR, for example the dissociation, diffusion and incorporation energy barriers, depend on the material surface structure.[4,11–20] An important example is Mastrikov *et al.*'s recent assessment, using DFT calculations, of the plausible pathways for oxygen incorporation into the $LaMnO_3$ (LMO) surface,[17] a widely studied cathode material. They identified that the rate determining steps (RDS) are the dissociation of the $O_2$ molecule to two adsorbed oxygen atoms, and the encounter of the surface oxygen vacancy and the adsorbed atomic oxygen by thermally activated diffusion of the vacancies or the dissociated oxygen atoms on the surface. Mastrikov *et al.* also suggested that these mechanisms are applicable to other transition metal oxide cathodes such as $LaFeO_3$ and $LaCoO_3$. From this, we can deduce that the diffusion of oxygen vacancies and of adsorbed/dissociated oxygen on the surface of SOFC cathodes, in part, governs the oxygen reduction kinetics, and thereby the cathode activity.

Lattice strain, for example induced by the lattice mismatch at the interface of a film and a substrate, was shown recently to have a significant impact on facilitating oxygen ion transport,[21–24] vacancy formation,[25–28] and surface adsorption.[26] Beyond these recent findings on strained SOFC oxides, the role of strain in altering the transport kinetics was also shown for dopant and atomic diffusion in other materials; examples include Si and Si–Ge alloys that are of importance to the semiconductor field,[29,30] $SiO_2$, a prototypical network-forming material,[31] and grain boundaries of MgO,[32] both studied in geosciences. On SOFC cathode materials, Sase *et al.* have reported an enhanced oxygen exchange and transport kinetics by ~3 orders of magnitude at the hetero-interface of (La,Sr)$CoO_3$ and (La,Sr)$_2CoO_{4+\delta}$ relative to the corresponding bulk values.[33] This enhancement could in part be attributed to the role of local distortions and strains to drive the ORR-related reactions near that interface. Using DFT calculations, we have recently demonstrated that the epitaxial strain up to a critical tensile strain value favors oxygen vacancy formation as well as oxygen adsorption on $LaCoO_3$,[26] and

*Laboratory for Electrochemical Interfaces, Department of Nuclear Science and Engineering, Massachusetts Institute of Technology, 77 Massachusetts Avenue, Cambridge, MA, 02139, USA. E-mail: byildiz@mit.edu*

oxygen vacancy formation and Sr segregation energies on (La,Sr)$MnO_3$.[28,34] We have also experimentally shown that the strain state in (La,Sr)$CoO_3$ films can induce different amounts of oxygen vacancies on the film surfaces.[35] These recent results showed that lattice strain can alter the thermodynamic stability of defects and adsorbed reactants on SOFC cathodes. It remains to be seen whether epitaxial strain can also directly drive the kinetics of oxygen reduction by altering the energy barriers of the governing ORR steps on SOFC cathodes.

In this paper, our purpose is to assess the mechanistic and quantitative effects of lattice strain on the diffusion of oxygen vacancy and adsorbed atomic oxygen on the surface of $LaCoO_3$ (LCO), another important perovskite oxide SOFC cathode. As we mentioned earlier, these processes facilitate the dissociation and incorporation of the adsorbed oxygen molecules in ORR.[17] We perform DFT calculations to provide an atomic scale view of oxygen transport and incorporation on strained LCO(001) surfaces. We first assess the rate-determining processes that are proposed to govern the overall oxygen incorporation kinetics. We then identify the effect of planar tensile strain on the migration energy barrier of those steps on LCO(001). We demonstrate that planar tensile lattice strain enhances one dimensional anisotropic mobility for oxygen vacancies on LCO (001) along the [1$\bar{1}$0] direction by reducing the migration energy barriers in that direction, and suppresses the migration in the [110] direction. Increasing tensile strain hinders the diffusion of adsorbed atomic oxygen. The governing mechanisms for these results and the overall assessment of the effect of strain on ORR kinetics on the LCO(001) surface are discussed.

## 2. Computational details

We performed plane wave DFT calculations using the Vienna *ab initio* simulation package (VASP).[36] We employed the generalized gradient approximation (GGA) parameterized by Perdew and Wang[37] along with the projector augmented wave (PAW)[38] method to describe ionic cores. To avoid the self-interaction errors that occur in the traditional DFT for strongly correlated electronic systems, we employed the DFT + $U$ method within Dudarev's approach[39] accounting for the on-site Coulomb interaction in the localized $d$ or $f$ orbitals. The spin state of the Co and the resulting configuration energies may be very sensitive to this $U$-correction term, so care must be given to the selection of a suitable $U$-correction value.[40,41] The correction parameter of effective $U$–$J$ = 3.3 eV was chosen with $J$ = 1 eV,[41] as previously determined by Wang *et al.*[40] by fitting the enthalpies of oxidation reactions. Recently, Kushima *et al.* have shown that this $U$–$J$ value is also applicable to describing $LaCoO_3$[26] and predicting the mechanism and energetics of oxygen transport in tetragonal $La_2CoO_{4+\delta}$.[42] All calculations used a plane wave expansion with a cutoff of 400 eV and included spin polarization. Geometries were relaxed using a conjugate gradient algorithm until the forces on all unconstrained atoms were less than 0.03 eV Å$^{-1}$.

The DFT-optimized cubic lattice constant is 3.83 Å, which is in good agreement with an experimental value of 3.80 Å.[43–45] To replicate the experimental epitaxial strain conditions that LCO thin films are subjected to on dissimilar substrates, a 2D-planar lattice strain was imposed by elongating the simulation cell in the $x$ and $y$ directions and relaxing the cell configuration and dimension in the $z$ direction. The bulk structure of $LaCoO_3$ was cleaved along the (001) plane to construct a surface that is represented by a slab of ~11.5 Å thick containing 7 atomic symmetric layers. The symmetric slab was chosen to avoid the fictitious dipole moment. We focused only on the $CoO_2$-terminated (001) which has been theoretically reported as the most stable in perovskite-type oxides[12,41,46] including LCO. For all calculations, a vacuum spacing of ~15 Å was placed in the direction of surface normal. As shown in Fig. 1, we have chosen a $2\sqrt{2} \times 2\sqrt{2}$ surface unit cell for minimizing the interactions between adsorbates or surface defects.[16,17,47] One oxygen vacancy or one oxygen adsorbate in the surface unit cell corresponds to an oxygen vacancy fraction or a surface coverage of 12.5%, respectively. The adsorbates and surface defects were placed on both sides of the slab to retain the symmetry. A 2 × 2 × 1 Monkhorst-Pack $k$-point mesh was used, which was sufficient to give well converged results.

The climbing image nudged elastic band (CI-NEB) method[48] was employed to calculate the migration barriers of both the oxygen vacancy and atomic oxygen as a function of planar strain on the LCO surface. Initial approximations to reaction paths were obtained by linear interpolation between the energy minima configurations. Three intermediate images were used for all NEB calculations, which were sufficient to map the minimum energy path (MEP) accurately. The NEB simulations were conducted with fixed lattice vectors.

## 3. Results and discussion

### A. Governing steps in the incorporation of $O_2$ into the unstrained LCO(001)

Mastrikov *et al.* suggested that five basic reaction steps on the surface are involved in the oxygen incorporation pathway into LMO(001): (1) $O_2$ adsorption, (2a) $O_2$ adsorption/incorporation into the surface oxygen vacancy, or (2b) $O_2$ dissociation without oxygen vacancy assistance, (3) migration of the oxygen vacancy (to the dissociated atomic oxygen), (4) migration of the dissociated atomic oxygen (to the oxygen vacancy), and (5) incorporation of the atomic oxygen into the oxygen vacancy on the surface.[17] Steps (1), (2a), and (5) were shown to be almost barrier-

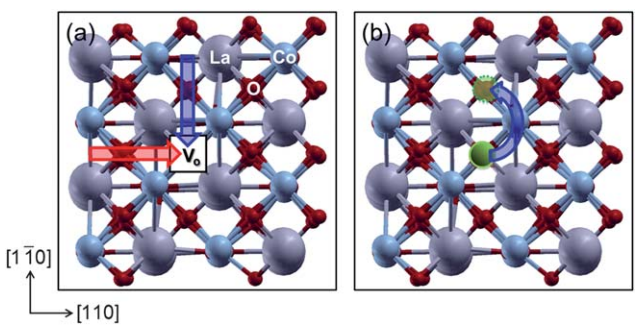


**Fig. 1** Top views of the $2\sqrt{2} \times 2\sqrt{2}$ $LaCoO_3$(001) surface unit cell that schematically shows (a) two diffusion pathways for oxygen vacancy, along the [1$\bar{1}$0] direction (blue arrow) and along the [110] direction (red arrow) and (b) the adsorbed atomic oxygen diffusion pathway on the surface, from atop an oxygen to the nearest neighbor oxygen through atop the Co.

free processes, rendering the steps (2b), (3), and (4) as the RDS of the oxygen incorporation pathway on LMO.[17] In order to identify the reactions governing the oxygen transport and incorporation kinetics on LCO(001), we also consider the above five reaction steps. We firstly observe that $O_2$ adsorption onto a Co cation on the surface (reaction step (1)) is thermodynamically favorable by 0.21 eV without an energy barrier. Our NEB calculations show that the reaction step (2a) is also barrier-free (Fig. 2(a)). In addition, incorporation of a dissociated atomic oxygen into an oxygen vacancy neighboring the adsorption site (reaction step (5)) is barrier-free and is thermodynamically favorable by 1.22 eV, as shown in Fig. 2(b). Therefore, reaction steps (1), (2a), and (5) lead to the $O_2$ dissociation with the assistance of an oxygen vacancy, and all are barrier-free processes on LCO(001).

The $O_2$ molecule adsorbs most favorably atop Co atom on defect-free LCO(001).[26] Our calculations here show that surface lattice oxygen is the most stable adsorption site for atomic oxygen on LCO(001) (this is equivalent to the $O_2$ molecular adsorption into a surface oxygen vacancy). For the $O_2$ dissociation reaction without vacancies, the surface with adsorbed $O_2$ on Co is more stable by 1.03 eV than the surface with two adsorbed atomic oxygen atoms on the lattice oxygen atoms (Fig. 2(c)). Other possible final states (i) with one dissociated atomic oxygen adsorbed on the same Co and the other on another nearest neighbor Co, and (ii) with one oxygen on the same Co and the other on the nearest neighbor surface oxygen were also investigated. Those final states are less stable by 0.51 and 0.29 eV, respectively, than the state with two adsorbed oxygen atoms on the lattice oxygen atoms. This suggests that the $O_2$ dissociation reaction without oxygen vacancy assistance on LCO(001) is thermodynamically unfavorable. It is unlike the case on the LMO(001) surface, which was shown to favor two dissociated and adsorbed atomic oxygen atoms in the final state by 1 eV compared to the initial state with one adsorbed $O_2$ on the Mn (Fig. 2(d)).[17] This dissimilar behavior between the LMO(001) and the LCO(001) may be related to the fact that the final favorable adsorption sites of adsorbed atomic oxygen differ on LMO and LCO; atop Mn atom on LMO(001),[17] and atop surface lattice oxygen on LCO(001). A more decisive reason for this difference between the reported results on LMO and our calculations on LCO might be the uncertainty of the accuracy of DFT calculations without the *U*-correction for LMO in Mastrikov *et al.*'s report. *U*-parameter is known to influence the adsorption energies and competition between different adsorption sites. For example, Lee *et al.* showed that the adsorption energy of atomic oxygen and its most favorable adsorption site on LMO(001) and LCO(001) vary significantly with the selected value of effective *U*.[41]

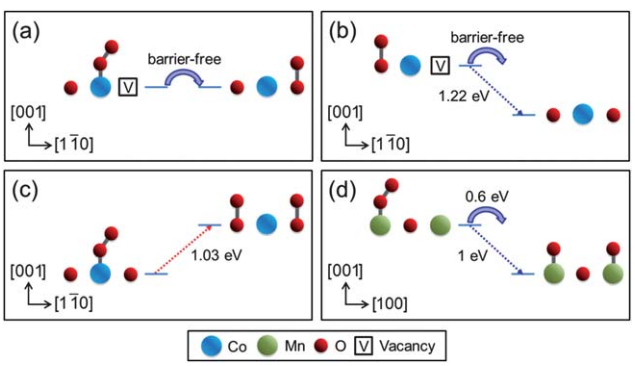


**Fig. 2** Reaction and energy diagram for (a) $O_2$ and (b) atomic oxygen incorporation into the surface oxygen vacancy, and for $O_2$ dissociation reaction without oxygen vacancy on (c) LCO(001) considered in this work, and on (d) LMO(001) from Mastrikov *et al.*'s results.[17]

Our result suggests that the $O_2$ molecule would not preferentially dissociate into two atomic oxygen atoms without the aid of a surface vacancy on LCO(001). We therefore rule out this unfavorable reaction step (2b) and the three barrier-free processes, steps (1), (2a), and (5), in further assessing the effects of strain, and focus on the migration of oxygen vacancy and adsorbed oxygen. For these two processes, the energy barriers are 0.70 eV and 0.17 eV, respectively, on the unstrained LCO (001), and their strain-response is assessed below.

### B. Anisotropic migration of oxygen vacancy on the strained LCO(001) surface

We first assess the effect of strain on the migration of oxygen vacancy along the [1$\bar{1}$0] direction on LCO(001) (Fig. 1(a)). Both the forward (F) and backward (B) paths in the [1$\bar{1}$0] direction were considered (Fig. 3(a)) due to the increase of asymmetry in the Co–O bond strength on the LCO surface with increasing strain. This is clear from the Co–O bond lengths in Fig. 3(b). Both the forward and the backward migration barriers along the [1$\bar{1}$0] direction decrease with increasing tensile strain quantitatively in a similar way (Fig. 3(a)), facilitating the vacancy mobility along this direction. The oxygen vacancy migration involves a curved path of an oxygen atom around the Co atoms, as shown in Fig. 4. This curved path of the migrating oxygen was also shown in previous experimental[49,50] and theoretical[15,51–54] reports in the bulk structure of various oxides, including perovskites as LCO, and alumina. Fig. 5 shows the vacancy migration process on the surface upon strain by mapping the electronic density distribution of the valence electrons describing the Co and O atoms near the migration path in the [1$\bar{1}$0] direction. Two metrics are evaluated to explain the decreasing migration barrier with increasing strain: the Co–O bond strength and the space available for the oxygen migration. The Co–O bond strengths, represented by the width of the charge density distribution between O and Co, from which the O detaches during migration. The bond strengths, shown by the yellow circles near (1) and (2), are almost similar in the initial state at $\varepsilon = 0.00$. With increasing strain, these bonds differ from each other—while (1) weakens, (2) strengthens. This is in agreement with the increasing Co–O bond length for (1) and the decreasing Co–O bond length for (2), shown in Fig. 3(b). While the bonds (1) and (2) differ in strength, both paths' migration barriers decrease the same amount with strain (Fig. 3(a)). On the other hand, the increasing space available for the oxygen migration correlates better with the decrease in the migration barrier at high strains. The wider space near the migration path in the saddle states (Fig. 5) with increasing planar tensile strain induces easier migration of oxygen atoms along the curved path around Co by lowering the migration barrier. Fig. 3(c) shows the space increase near the migration path in the [1$\bar{1}$0] direction, measured as the Co–Co

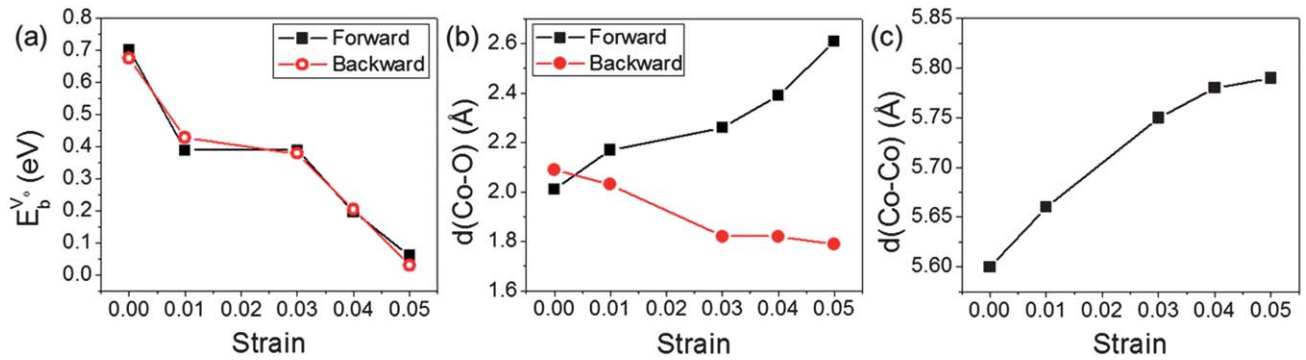


**Fig. 3** (a) Migration energy barrier of oxygen vacancy along the forward and backward paths in the [1$\bar{1}$0] direction of the LCO(001) surface, (b) the change in the Co–O distance (shown with the yellow circles (1) and (2) in Fig. 5) at the initial state, and (c) the change in the Co–Co distance (shown with the white arrow in Fig. 5) at the saddle state in the [1$\bar{1}$0] direction, as a function of planar tensile strain from 0.00 to 0.05. Increase in the migration space, *d*(Co–Co), correlates well with the decrease of the migration barrier in (a).

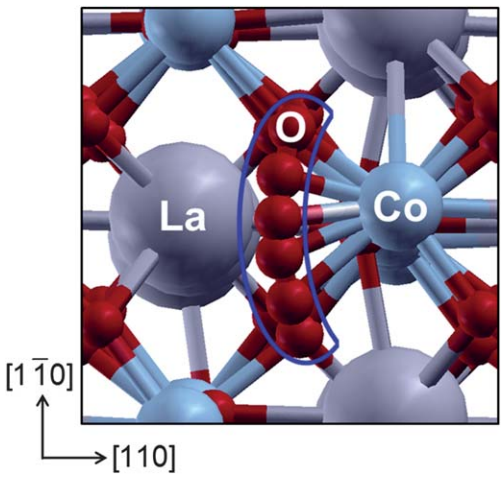


**Fig. 4** The curved path of an oxygen atom around the Co atoms for the vacancy migration on the LCO(001) surface.

bond length. The position of the Co–Co bond is shown by a white arrow in Fig. 5. The increase in the Co–Co bond length with increasing strain correlates well with the same decrease in the migration barrier for both paths. This implies that the space available to migrate a lattice oxygen atom (*via* exchange with a vacancy) is a more decisive factor in inducing higher mobility on the LCO surface than the Co–O bond strength that hinders the oxygen migration.

On the other hand, the migration of oxygen vacancy along the [110] direction is hindered with increasing strain. There are two types of the lattice oxygen rows on LCO(001) as seen in Fig. 6(a): one type (row 1) is lower than the other (row 2) in the [001] direction. In other words, the row 1 is suppressed into the surface while the row 2 is protruding out of the surface. The hindrance of the oxygen vacancy migration along the [110] direction is because the oxygen vacancy becomes less stable on row 1, the suppressed lattice oxygen sites, compared to that on row 2, the protruding sites. We assess this instability in terms of the asymmetry of the $CoO_6$ octahedral tilting on the surface of LCO. The $CoO_6$ octahedral distortion from the perfect cubic structure in LCO was well identified from high-resolution neutron powder diffraction measurements in the temperature range of 5 to 1000 K.[43] As shown in Fig. 6(a), the tilting angle of $CoO_6$, $\alpha$, shows the deviation of the octahedra from the perfect cubic structure (in which $\alpha = 0°$) and represents the surface anisotropy.[55–57] Increasing $CoO_6$ tilt induces increasing differences between the nature of oxygens on rows 1 and 2. The planar tensile strain increases the octahedral tilt, thereby the surface structure anisotropy, as shown by the increase of $\alpha$ in Fig. 6(b). The increase of $\alpha$ protrudes the row 2 more upwards, increasing the discrepancy between row 1 and row 2. Oxygen vacancy is therefore energetically more expensive to form on the suppressed row 1 with increasing strain. In fact, our calculations showed that the oxygen vacancies created on the suppressed oxygen sites on row 1 automatically relax to the protruding sites on row 2 during the fully relaxed structural optimization. We quantified the increase in the instability of vacancy on row 1 in terms of the formation energy difference ($\Delta E_{vac}$) between vacancy on row 1 and on row 2. To prevent the spontaneous oxygen vacancy relaxation to the row 2, we fixed the surface top layer in the (001) plane and relaxed only in the [001] direction with the oxygen vacancy on row 1. $\Delta E_{vac}$ in Fig. 6(b) increases with increasing tensile strain, implying that the formation of vacancy in the row 1 becomes increasingly harder.

Overall, such anisotropic diffusion of oxygen arises from the inherent anisotropy of the surface structure.[58] The surface diffusion of oxygen vacancies becomes more anisotropic at the higher strains, and favors to migrate along row 2 instead of across rows 1 and 2. As a result, the enhanced mobility of oxygen vacancies along the [1$\bar{1}$0] direction is accompanied by a suppressed mobility of vacancies along the [110] direction on the LCO surface when tensile strained on its (001) plane. This combination brings up the possibility of fast and anisotropic one dimensional mobility of oxygen vacancies on the LCO surface.

Similar to this one dimensional surface diffusion of oxygen vacancies driven by the anisotropic surface structure, the anisotropy of bulk oxygen diffusion has also been demonstrated for layered anisotropic oxide structures.[59–61] Particularly for the surfaces of cubic-like oxides, only recently such anisotropy in oxygen diffusion was observed on a strained rutile $TiO_2$(110) surface.[22] For that system, the diffusion of the bridging vacancy along the [001] and [1$\bar{1}$0] directions becomes more anisotropic with increasing strain applied along [1$\bar{1}$0].

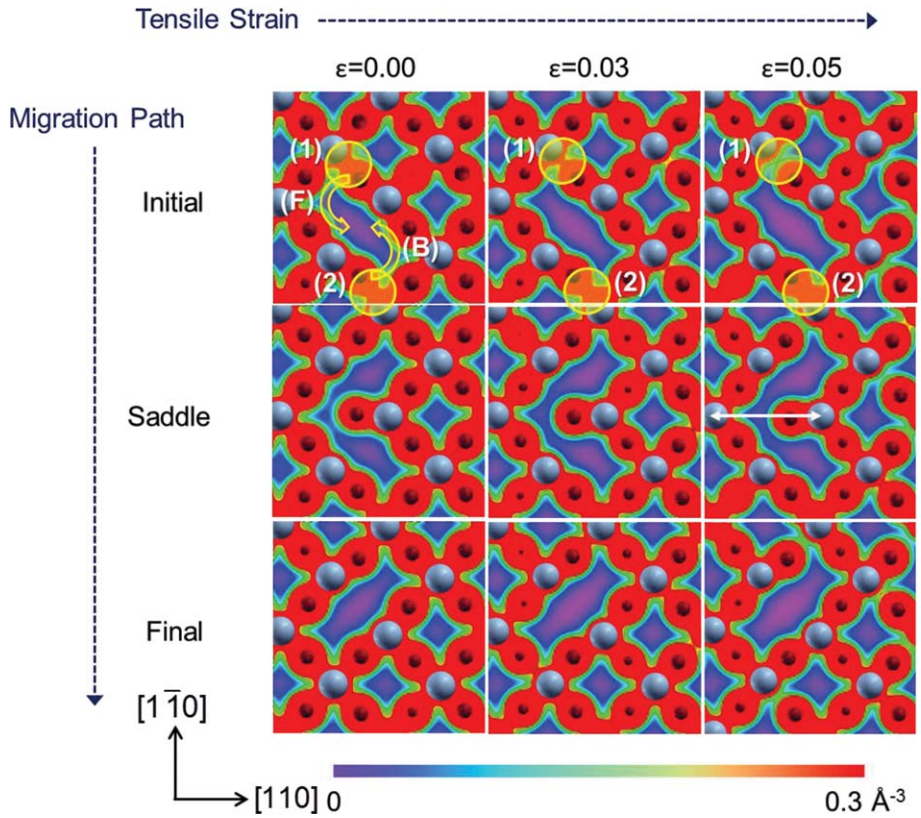


**Fig. 5** Electronic charge density distribution of oxygen vacancy migration on the LCO(001) plane as a function of planar tensile strain. The initial, saddle point, and final configurations along the forward (F) and backward (B) path in the [1$\bar{1}$0] direction are shown. Gray and red spheres represent Co and O atoms, respectively. The numbers (1) and (2) correspond to the bond lengths used in Fig. 3(b).

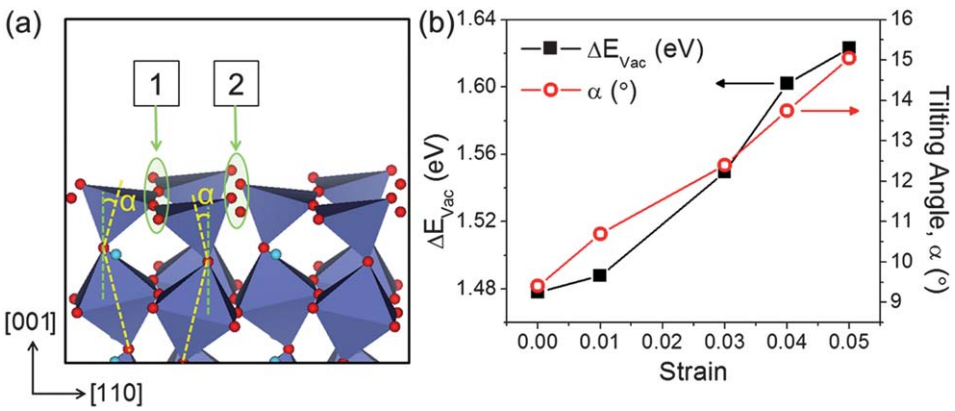


**Fig. 6** (a) Side view of the defect-free LCO(001) surface under 5% strain, showing the $CoO_6$ octahedral structure. Each octahedron is tilted by $\alpha$, protruding oxygen atoms on row 2 and suppressing them on row 1. Light blue and red spheres represent La and O atoms, respectively. (b) Oxygen vacancy formation energy difference between the row 1 and row 2, $\Delta E_{vac}$, and the tilt angle of $CoO_6$, $\alpha$, that represents the surface structure anisotropy as a function of strain. By our definition, a more positive $\Delta E_{vac}$ favors the formation of vacancy on row 2 over that on row 1.

### C. Migration of adsorbed atomic oxygen on the strained LCO(001) surface

As mentioned in Section 3A, the most stable adsorption site for atomic oxygen is the top of surface lattice oxygen on LCO(001). We therefore investigate a pathway in which the adsorbed oxygen migrates from atop one surface oxygen to atop the nearest neighbor oxygen as shown in Fig. 1(b). Our minimum energy path calculations using NEB for the adsorbed oxygen diffusion showed that the saddle point of migration is actually the same as the adsorption of oxygen atop Co atom. The calculated migration barrier of this path and the adsorption energy difference ($\Delta E_{ads}$) between adsorption on oxygen and on Co are within 0.05 eV. This confirms that the migration of adsorbed oxygen passes from atop Co. For computational efficiency, we therefore take the migration barrier of adsorbed atomic oxygen, $E_b^{\text{atomic O}}$ as equivalent to the $\Delta E_{ads}$. The migration barriers in both the [110] and [1$\bar{1}$0] directions do not differ,

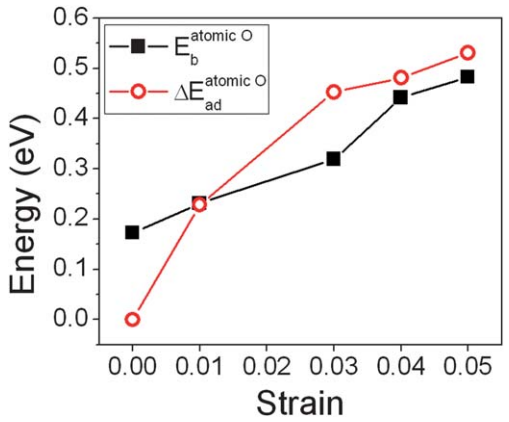


**Fig. 7** The migration energy barrier ($E_b^{atomic\ O}$) and the relative adsorption energy ($\Delta E_{ad}^{atomic\ O}$) of adsorbed atomic oxygen as a function of strain. The migration path is shown in Fig. 1(b).

because the adsorption energies of atomic oxygen on row 1 and row 2 are similar (within 0.14 eV) and both diffusion paths go through the same Co atom (saddle point). Therefore, we focus only on the [1$\bar{1}$0] path, as shown in Fig. 1(b). The migration barrier of atomic oxygen adsorbate on LCO(001) increases with increasing strain (Fig. 7). This trend is opposite to that of the decreasing migration barrier of oxygen vacancy along the [1$\bar{1}$0]. We recently showed that, for the LCO(001) surface, increasing planar tensile strain weakens the in-plane Co–O bonds (by decreasing the Co *d* and lattice O *p* orbitals' hybridization), which consequently causes to strengthen the adsorption of $O_2$ onto Co.[26] Here this weakening of the lattice Co–O bonds also induces the atomic oxygen to be adsorbed more strongly atop the surface lattice oxygen of LCO(001). Fig. 7 shows the relative increase of the adsorption energy for atomic oxygen ($\Delta E_{ad}^{atomic\ O}$) with increasing strain. By this strengthening mechanism, the increasing tensile strain hinders the dissociative migration of the adsorbed oxygen.

## 4. Conclusion

We demonstrated and assessed the competing effects of planar strain on the oxygen incorporation mechanism on the LCO(001) surface using DFT + *U* calculations. The migrations of oxygen vacancy and of adsorbed atomic oxygen are identified as the key RDS that govern the overall incorporation kinetics on the LCO (001) $CoO_2$ surface. Planar tensile strain induces an enhanced one dimensional anisotropic mobility for oxygen vacancy along the [1$\bar{1}$0] by reducing the migration energy barrier, while suppressing diffusion along the [110] direction. The reason for the increased uni-directional mobility is the increasing asymmetric tilt of the $CoO_6$ octahedra at high tensile strains. This destabilizes the oxygen vacancy formation at the suppressed surface oxide rows of LCO(001), blocking the migration paths which go through those sites in the [110] direction. The diffusion of adsorbed O, on the other hand, is hindered at increasing tensile strain because of the enhanced adsorption strength of the atomic oxygen.

Given such competing effects of strain, a reasonable question to ask is "what is the optimal strain for maximal enhancement of ORR kinetics, if any?" A precise answer to this question requires the assessment of the collective kinetic behavior of the surface reactions, formulated in the framework of transition state theory and computed *via* kinetic Monte Carlo simulations, in a similar way that we identified the "*fastest* strain" in YSZ.[21] Those simulations take as input all the unit process energetics that are assessed in this paper, and this is part of our future work. Here we provide only an approximate estimation of the "winner" among the enhanced one-dimensional mobility of vacancies, the suppression of a vacancy migration path, and the suppression of the adsorbed oxygen migration with increasing strain. For this we compare the strain dependence of the collective oxygen vacancy diffusion (that depends on the vacancy formation and vacancy mobility) and the collective adsorbed oxygen diffusion (that depends on the adsorption coverage and oxygen mobility).

The ratios of the oxygen vacancy diffusivity ($\upsilon$) and of the adsorbed oxygen diffusivity ($O$) on the strained surface to that on the unstrained surface can be estimated by:

$$\frac{D_S^{st}}{D_S^{unst}} \approx \frac{C_S^{st} d_S^{st}}{C_S^{unst} d_S^{unst}} \approx \frac{e^{\left(-E_{c_{st}}^S/kT\right)} e^{\left(-E_{d_{st}}^S/kT\right)}}{e^{\left(-E_{c_{unst}}^S/kT\right)} e^{\left(-E_{d_{unst}}^S/kT\right)}} = e^{\left\{-\left(\Delta E_c^S + \Delta E_d^S/kT\right)\right\}} \quad (1)$$

where st and unst denote the strained and unstrained states, S stands for $\upsilon$ or $O$, $D_S^{st}$ and $D_S^{unst}$ denote the diffusion coefficients of vacancy or adsorbed oxygen, $C_S^{st}$ and $C_S^{unst}$ denote the vacancy concentration fractions or the adsorption coverages of oxygen, $d_S^{st}$ and $d_S^{unst}$ denote the diffusivities of single vacancy or adsorbed oxygen, $E_{c_{st}}^S$ and $E_{c_{unst}}^S$ the vacancy formation or $O_2$ adsorption energies, $E_{d_{st}}^S$ and $E_{d_{unst}}^S$ the migration barriers of oxygen vacancy or adsorbed atomic oxygen, and $\Delta E_c^S = E_{c_{st}}^S - E_{c_{unst}}^S$ and $\Delta E_d^S = E_{d_{st}}^S - E_{d_{unst}}^S$ the energy difference between the strained and unstrained LCO(001). $k$ is the Boltzmann constant and $T$ is the temperature. Here, to a first order approximation, we assume that the prefactor terms that multiply the exponential terms are approximately independent of strain.

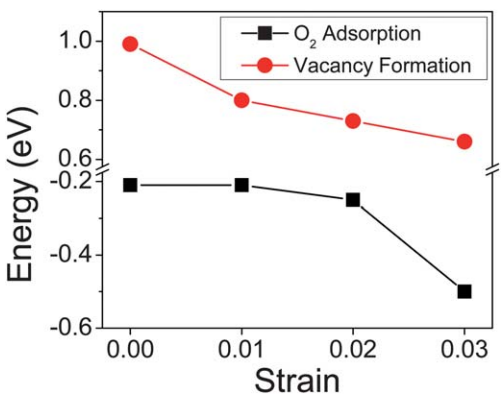


**Fig. 8** Tensile planar strain dependence of the $O_2$ adsorption (atop a surface Co cation) and oxygen vacancy formation energies on the LCO (001) surface. By our definition, a more negative $O_2$ adsorption energy favors the adsorption of the $O_2$ molecule more strongly, and a less oxygen vacancy formation energy corresponds to the easier formation of vacancy on the surface.

We choose 3% planar tensile strain to determine the effective increase or decrease of ORR activity on LCO(100). We previously reported the vacancy formation and adsorption energy on LCO(100) as a function of strain.[26] However, since ref. 26 used smaller unit cells than those used in this study, here we recalculated the strain-dependence of these energies with unit cell and calculation parameters that are consistent with all those in this paper, and the results are shown in Fig. 8. At 3% strain, the oxygen vacancy formation energy decreases by 0.32 eV and $O_2$ adsorption is strengthened by 0.29 eV compared to the strain-free surface. Then according to eqn (1), surface oxygen vacancy diffusion at 3% strain is more facile than at the strain-free state by $\Delta E_c^v + \Delta E_d^v = -0.62$ eV ($\Delta E_c^v = -0.32$ eV from oxygen vacancy formation energy, and $\Delta E_d^v = -0.30$ eV from the energy barrier of oxygen vacancy migration along the [1$\bar{1}$0] in Fig. 3(a)). Planar tensile strain also suppresses the two dimensional mobility of oxygen vacancy and shifts the diffusion to a uni-directional path. Based on the results in Fig. 6(b), 3% strain makes [110] directional diffusion of oxygen vacancy 0.07 eV harder than on the unstrained surface. If we simply incorporate this relative reduction of vacancy diffusion by linearly accounting for the barriers, $\Delta E_d^v$ becomes −0.23 eV, so $\Delta E_c^v + \Delta E_d^v = -0.55$ eV. This corresponds to the three orders of magnitude ($\times 10^3$) enhanced oxygen diffusion on the LCO(001) surface compared to the unstrained LCO(001) at 550 °C. In a similar way, atomic oxygen diffusion on the 3% strained surface would be more facile by $\Delta E_c^O + \Delta E_d^O = -0.14$ eV ($\Delta E_c^O = -0.29$ eV from $O_2$ adsorption which would increase the $O_2$ presence on the surface, and $\Delta E_d^O = +0.15$ eV from the energy barrier of atomic oxygen (Fig. 7)) than on the strain-free surface. This corresponds to enhanced oxygen adsorbate diffusion by one order of magnitude ($\times 10^1$) compared to the unstrained LCO(001) at 550 °C. From the comparison of these energetics, we predict that strain (up to 3%) enhances the oxygen vacancy diffusion (by −0.55 eV) more dominantly than the atomic oxygen diffusion (by −0.14 eV), effectively increasing the surface oxygen diffusion by approximately three orders of magnitude.

While a more accurate and quantitative assessment of the strain response of the collective behavior of these processes in oxygen incorporation kinetics is warranted, from this estimate, we expect that the significantly lower energy barrier for oxygen vacancy diffusion would dominate the other degrading factors and actually accelerate the ORR kinetics on LCO(001) up to 3% strain. Furthermore, the insights obtained here are useful for designing strategies to control the desired anisotropic and uni-directional oxygen transport along strained hetero-interfaces on the surfaces.

## Acknowledgements

Authors acknowledge Sidney Yip at MIT for helpful discussions, the US-DOE—Basic Energy Sciences, Grant No DE-SC0002633 for financial support, and the National Science Foundation for computational support through the TeraGrid Advanced Support Program, Grant No TG-ASC090058.

## References

1 B. C. H. Steele and A. Heinzel, *Nature*, 2001, **414**, 345.
2 A. J. Jacobson, *Chem. Mater.*, 2010, **22**, 660.
3 A. Tarancon, M. Burriel, J. Santiso, S. J. Skinner and J. A. Kilner, *J. Mater. Chem.*, 2010, **20**, 3799.
4 A. Chroneos, B. Yildiz, A. Tarancon, D. Parfitt and J. A. Kilner, *Energy Environ. Sci.*, 2011, **4**, 2774.
5 R. J. Chater, S. Carter, J. A. Kilner and B. C. H. Steele, *Solid State Ionics*, 1992, **53–56**, 859.
6 R. A. De Souza and J. A. Kilner, *Solid State Ionics*, 1998, **106**, 175.
7 R. De Souza, *Phys. Chem. Chem. Phys.*, 2006, **8**, 890.
8 D. Mori, H. Oka, Y. Suzuki, N. Sonoyama, A. Yamada, R. Kanno, Y. Sumiya, N. Imanishi and Y. Takeda, *Solid State Ionics*, 2006, **177**, 535.
9 A. Yamada, Y. Suzuki, K. Saka, M. Uehara, D. Mori, R. Kanno, T. Kiguchi, F. Mauvy and J.-C. Grenier, *Adv. Mater.*, 2008, **20**, 4124.
10 M. Liu and H. Hu, *J. Electrochem. Soc.*, 1996, **143**, L109.
11 Y. Choi, M. Lin and M. Liu, *Angew. Chem., Int. Ed.*, 2007, **46**, 7214.
12 Y. Choi, D. S. Mebane, M. C. Lin and M. L. Liu, *Chem. Mater.*, 2007, **19**, 1690.
13 Y. Choi, D. Mebane, J.-H. Wang and M. Liu, *Top. Catal.*, 2007, **46**, 386.
14 Y. Choi, M. E. Lynch, M. C. Lin and M. Liu, *J. Phys. Chem. C*, 2009, **113**, 7290.
15 Y. Choi, M. C. Lin and M. Liu, *J. Power Sources*, 2010, **195**, 1441.
16 E. A. Kotomin, Y. A. Mastrikov, E. Heifetsa and J. Maier, *Phys. Chem. Chem. Phys.*, 2008, **10**, 4644.
17 Y. A. Mastrikov, R. Merkle, E. Heifets, E. A. Kotomin and J. Maier, *J. Phys. Chem. C*, 2010, **114**, 3017.
18 Y. A. Mastrikov, M. M. Kuklja, E. A. Kotomin and J. Maier, *Energy Environ. Sci.*, 2010, **3**, 1544.
19 H.-T. Chen, P. Raghunath and M. C. Lin, *Langmuir*, 2011, **27**, 6787.
20 E. A. Kotomin, Y. A. Mastrikov, M. M. Kuklja, R. Merkle, A. Roytburd and J. Maier, *Solid State Ionics*, 2011, **188**, 1.
21 A. Kushima and B. Yildiz, *J. Mater. Chem.*, 2010, **20**, 4809.
22 Z.-W. Wang, D.-J. Shu, M. Wang and N.-B. Ming, *Phys. Rev. B: Condens. Matter Mater. Phys.*, 2010, **82**, 165309.
23 N. Schichtel, C. Korte, D. Hesse and J. Janek, *Phys. Chem. Chem. Phys.*, 2009, **11**, 3043.
24 J. Garcia-Barriocanal, A. Rivera-Calzada, M. Varela, Z. Sefrioui, E. Iborra, C. Leon, S. J. Pennycook and J. Santamaria, *Science*, 2008, **321**, 676.
25 D.-J. Shu, S.-T. Ge, M. Wang and N.-B. Ming, *Phys. Rev. Lett.*, 2008, **101**, 116102.
26 A. Kushima, S. Yip and B. Yildiz, *Phys. Rev. B: Condens. Matter Mater. Phys.*, 2010, **82**, 115435.
27 W. Donner, C. Chen, M. Liu, A. J. Jacobson, Y.-L. Lee, M. Gadre and D. Morgan, *Chem. Mater.*, 2011, **23**, 984.
28 H. Jalili, J. W. Han, Y. Kuru, Z. Cai and B. Yildiz, *J. Phys. Chem. Lett.*, 2011, **2**, 801.
29 M. J. Aziz, *Appl. Phys. Lett.*, 1997, **70**, 2810.
30 M. J. Aziz, Y. Zhao, H.-J. Gossmann, S. Mitha, S. P. Smith and D. Schiferl, *Phys. Rev. B: Condens. Matter Mater. Phys.*, 2006, **73**, 054101.
31 M. J. Aziz, S. Circone and C. B. Agee, *Nature*, 1997, **390**, 596.
32 D. J. Harris, G. W. Watson and S. C. Parker, *Phys. Rev. B: Condens. Matter Mater. Phys.*, 2001, **64**, 134101.
33 M. Sase, K. Yashiro, K. Sato, J. Mizusaki, T. Kawada, N. Sakai, K. Yamaji, T. Horita and H. Yokokawa, *Solid State Ionics*, 2008, **178**, 1843.
34 J. W. Han, H. Jalili, Y. Kuru, Z. Cai and B. Yildiz, *ECS Trans.*, 2011, **35**, 2097.
35 Z. Cai, Y. Kuru, J. W. Han, Y. Chen and B. Yildiz, *J. Am. Chem. Soc.*, 2011, DOI:10.1021/ja2059445.
36 G. Kresse and J. Furthmuller, *Phys. Rev. B: Condens. Matter Mater. Phys.*, 1996, **54**, 11169.
37 J. P. Perdew, J. A. Chevary, S. H. Vosko, K. A. Jackson, M. R. Pederson, D. J. Singh and C. Fiolhais, *Phys. Rev. B: Condens. Matter Mater. Phys.*, 1992, **46**, 6671.
38 P. E. Blöchl, *Phys. Rev. B: Condens. Matter Mater. Phys.*, 1994, **50**, 17953.
39 S. L. Dudarev, G. A. Botton, S. Y. Savrasov, C. J. Humphreys and A. P. Sutton, *Phys. Rev. B: Condens. Matter Mater. Phys.*, 1998, **57**, 1505.
40 L. Wang, T. Maxisch and G. Ceder, *Phys. Rev. B: Condens. Matter Mater. Phys.*, 2006, **73**, 195107.
41 Y.-L. Lee, J. Kleis, J. Rossmeisl and D. Morgan, *Phys. Rev. B: Condens. Matter Mater. Phys.*, 2009, **80**, 224101.

42 A. Kushima, D. Parfitt, A. Chroneos, B. Yildiz, J. A. Kilner and R. W. Grimes, *Phys. Chem. Chem. Phys.*, 2011, **13**, 2242.
43 P. G. Radaelli and S. W. Cheong, *Phys. Rev. B: Condens. Matter Mater. Phys.*, 2002, **66**, 094408.
44 D. Fuchs, E. Arac, C. Pinta, S. Schuppler, R. Schneider and H. V. Löhneysen, *Phys. Rev. B: Condens. Matter Mater. Phys.*, 2008, **77**, 014434.
45 V. V. Mehta, M. Liberati, F. J. Wong, R. V. Chopdekar, E. Arenholz and Y. Suzuki, *J. Appl. Phys.*, 2009, **105**, 07E503.
46 R. A. Evarestov, E. A. Kotomin, Y. A. Mastrikov, D. Gryaznov, E. Heifets and J. Maier, *Phys. Rev. B: Condens. Matter Mater. Phys.*, 2005, **72**, 214411.
47 J. Fleig, R. Merkle and J. Maier, *Phys. Chem. Chem. Phys.*, 2007, **9**, 2713.
48 G. Henkelman, B. P. Uberuaga and H. Jónsson, *J. Chem. Phys.*, 2000, **113**, 9901.
49 M. Yashima, K. Nomura, H. Kageyama, Y. Miyazaki, N. Chitose and K. Adachi, *Chem. Phys. Lett.*, 2003, **380**, 391.
50 M. M. Günter, H. Boysen, C. Corte, M. Lerch and E. Suard, *Z. Kristallogr.*, 2005, **220**, 218.
51 M. S. Islam, M. Cherry and C. R. A. Catlow, *J. Solid State Chem.*, 1996, **124**, 230.
52 M. S. Islam, *J. Mater. Chem.*, 2000, **10**, 1027.
53 M. S. Islam, *Solid State Ionics*, 2002, **154–155**, 75.
54 U. Aschauer, P. Bowen and S. C. Parker, *Acta Mater.*, 2009, **57**, 4765.
55 A. T. Zayak, X. Huang, J. B. Neaton and K. M. Rabe, *Phys. Rev. B: Condens. Matter Mater. Phys.*, 2006, **74**, 094104.
56 S. J. May, J. W. Kim, J. M. Rondinelli, E. Karapetrova, N. A. Spaldin, A. Bhattacharya and P. J. Ryan, *Phys. Rev. B: Condens. Matter Mater. Phys.*, 2010, **82**, 014110.
57 A. Vailionis, H. Boschker, W. Siemons, E. P. Houwman, D. H. A. Blank, G. Rijnders and G. Koster, *Phys. Rev. B: Condens. Matter Mater. Phys.*, 2011, **83**, 064101.
58 T. Ala-Nissila, R. Ferrando and S. C. Ying, *Adv. Phys.*, 2002, **51**, 949.
59 S. Inoue, M. Kawai, N. Ichikawa, H. Kageyama, W. Paulus and Y. Shimakawa, *Nat. Chem.*, 2010, **2**, 213.
60 E. Kendrick, J. Kendrick, K. S. Knight, M. S. Islam and P. R. Slater, *Nat. Mater.*, 2007, **6**, 871.
61 A. Chroneos, D. Parfitt, J. A. Kilner and R. W. Grimes, *J. Mater. Chem.*, 2010, **20**, 266.

 